Supporting Information

Validation of Human Sterol 14α-Demethylase (CYP51) Druggability: Structure-Guided Design, Synthesis and Evaluation of Stoichiometric, Functionally Irreversible Inhibitors

Laura Friggeri,[†] Tatiana Y. Hargrove,[†] Zdzislaw Wawrzak,[§] F. Peter Guengerich[†], and Galina I. Lepesheva*[,†,‡,ᵗ]

[†]*Department of Biochemistry, Vanderbilt University School of Medicine, Nashville, Tennessee 37232, USA*

[§]*Synchrotron Research Center, Life Science Collaborative Access Team, Northwestern University, Argonne, Illinois 60439, USA*

[‡]*Center for Structural Biology, Vanderbilt University, Nashville, Tennessee 37232, USA*

[ᵗ]*Vanderbilt-Ingram Cancer Center, Nashville, Tennessee 37232, USA*

Contents of Supporting Information

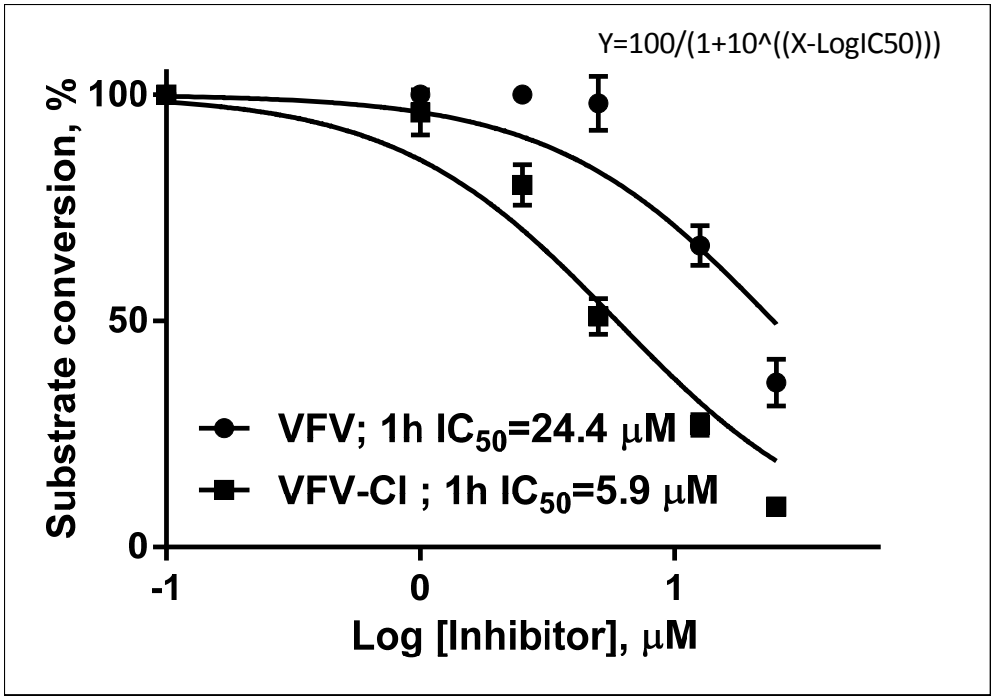

Supporting Figure S1. Inhibitory effects of VFV and VFV-Cl on human CYP51 activity. The reaction time was 60 min. Fit to log [inhibitor] vs. normalized response, nonlinear regression (GraphPad Prism 6). Inset formula form Prism. The P450 concentration was 0.5 μM, the lanosterol concentration was 50 μM, and the concentration range of the inhibitors was 1-25 μM. Graph represents mean ± SD of two independent experiments in duplicate.

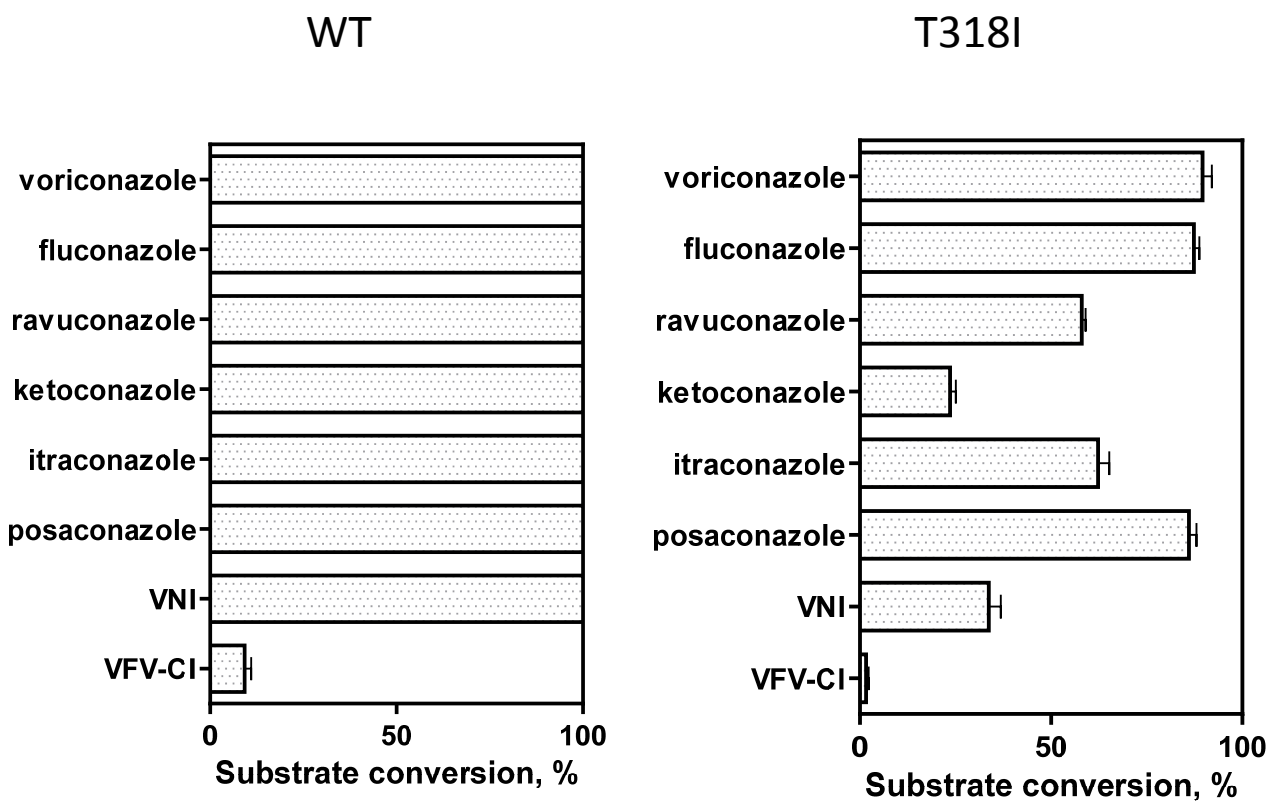

Supporting Figure S2. **The T318I mutation increases susceptibility of human CYP51 to inhibition.** The reaction time was 60 min, the P450 concentration was 0.5 µM, the inhibitor/enzyme molar ratio was 50/1, and the lanosterol concentration was 50 µM. Graphs represent mean ± SD of two independent experiments in duplicate.

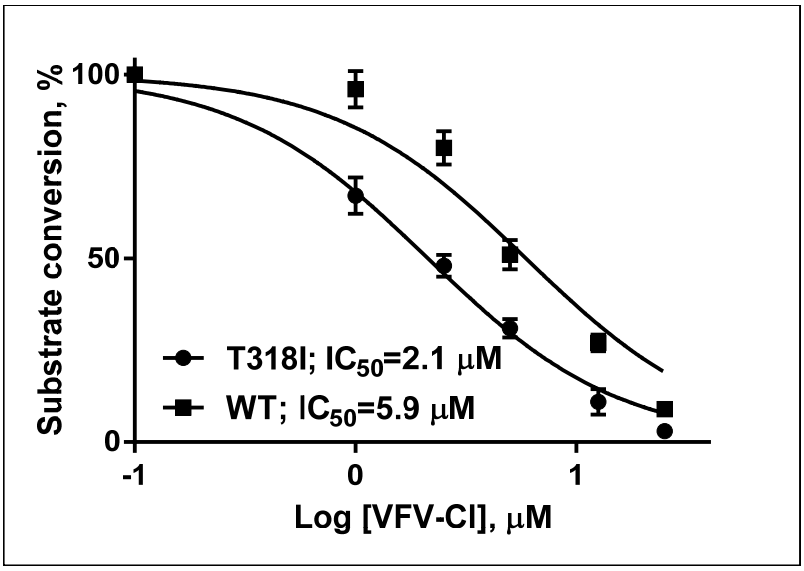

Supporting Figure S3. Inhibitory effects of VFV-Cl on the activity of the T318I and WT human CYP51. The reaction time was 60 min. Fit to log [inhibitor] vs. normalized response, nonlinear regression (GraphPad Prism 6) P450 concentration was 0.5 μM, the lanosterol concentration was 50 μM, and the concentration range of the inhibitors was 1-25 μM. The graph represents mean ± SD of two independent experiments in duplicate.

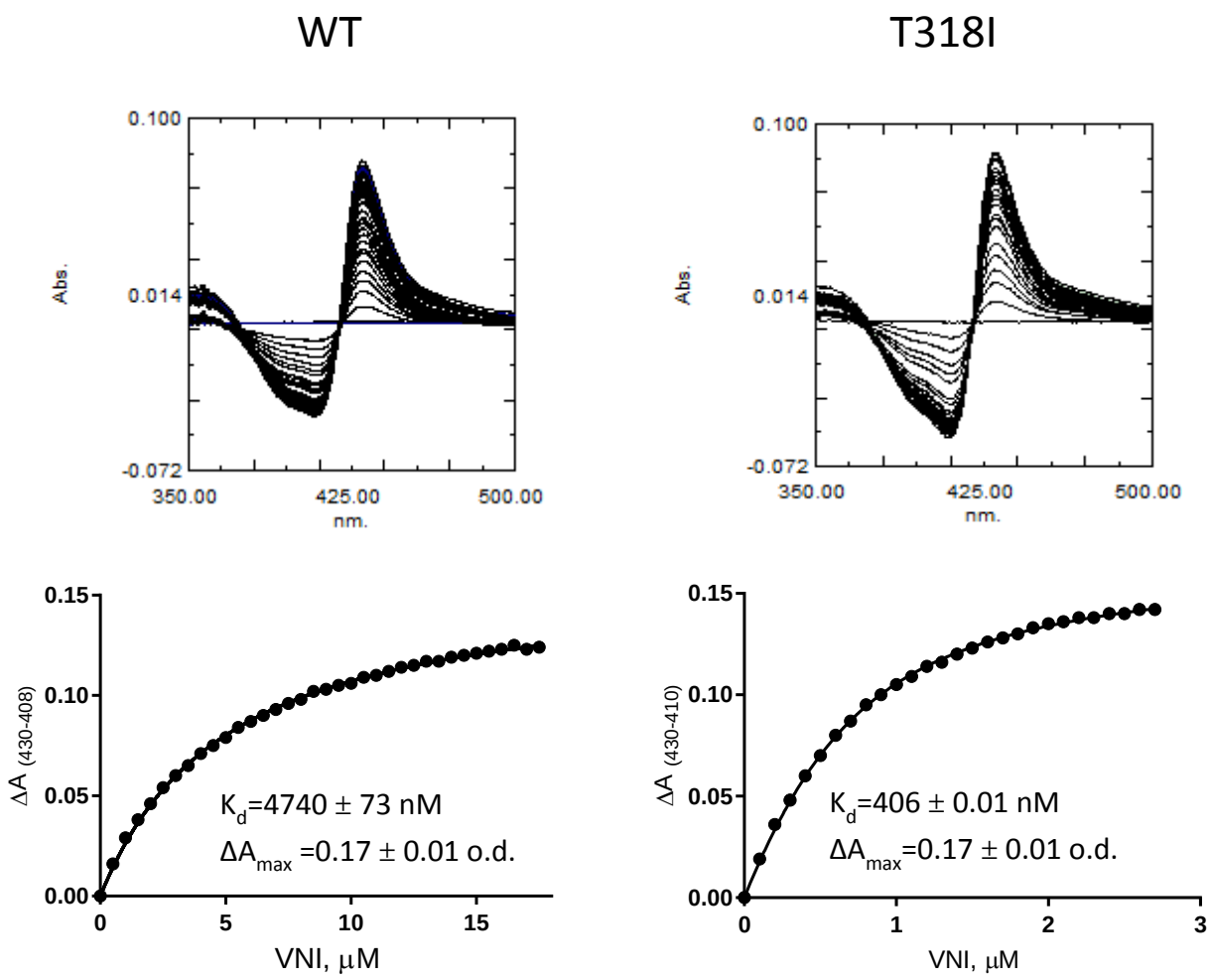

Supporting Figure S4. **The T318A mutation increases the binding affinity of human CYP51 to VNI.** Top: difference absorbance spectra upon titration with VNI; bottom: titration curves (fit to Morrison equation, nonlinear regression), optical path length 5 cm, P450 concentration 0.5 μM. For the WT the titration range was 0.5-17.5 μM and the titration step was 0.5 μM. For the T318I mutant the titration range was 0.1-2.5 μM, the titration step was 0.1 μM.

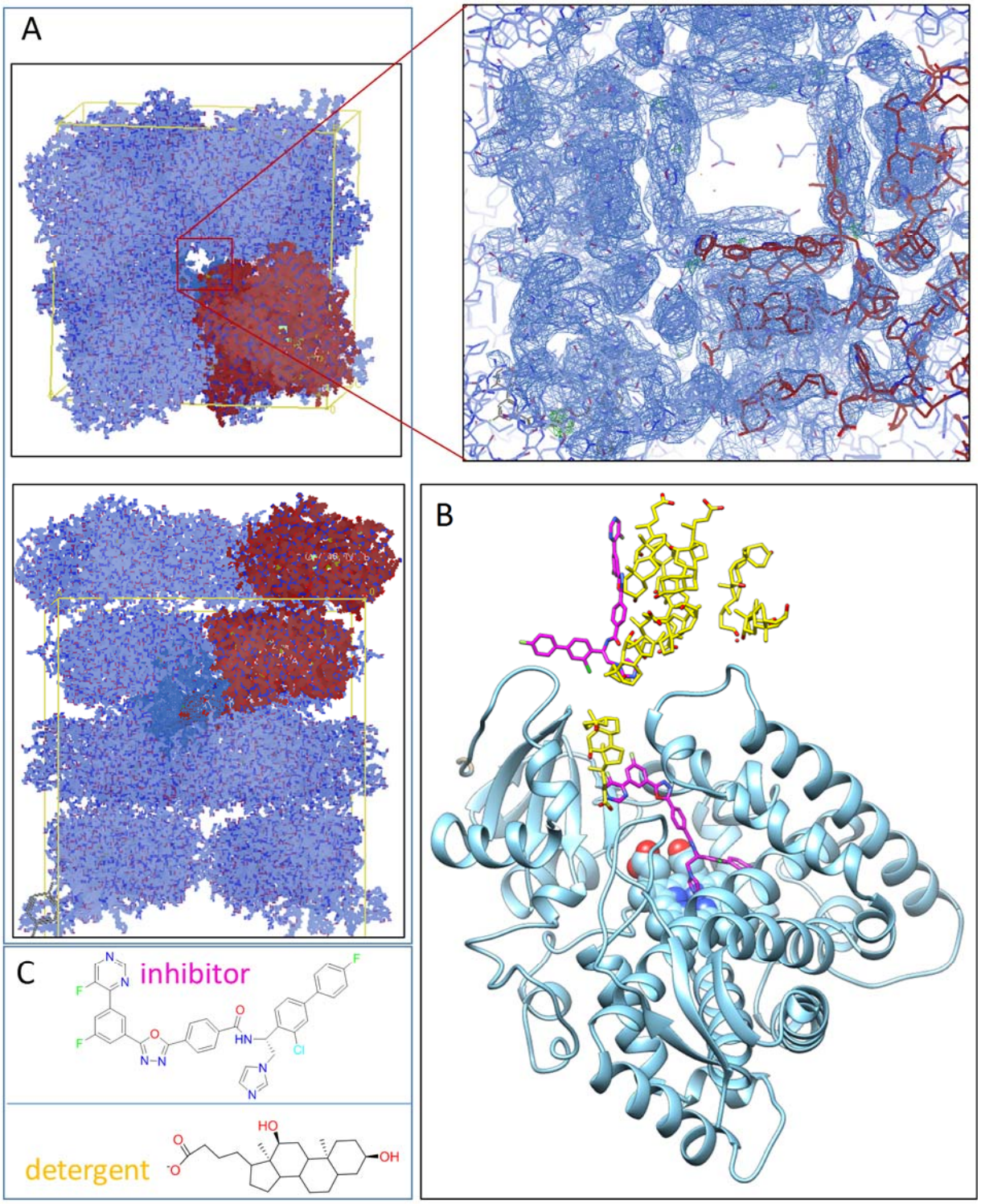

Supporting Figure S5. X-ray structure of human CYP51 co-crystallized with compound 10. A. Unit cell. Two molecules forming an asymmetric unit are colored in red. Inset: the enlarged view of the channel. B. Overall (distal P450) view of one CYP51 molecule with 2 molecules of compound **10** (magenta) and 8 molecules of the detergent (yellow). **C**. Structural formulas.

Table S1. Ligand-contacting residues (≤4.5 Å) in human CYP51 complexes/, the model and the structures.

CYP51 secondary structural element	Ligand		
	Model: compound **10-A/** compound **10-B**	Structure 4uhi: VFV-A/ VFV-B	Structure 6Q2T: compound **10**/ detergent
A’	– / L71, F77	–/ L71, F77	– / L71, A74, I75, F77, G78
β1-1turn β1-2turn	– / F98, M100, V101 F105/ F105,Y107	– / F98, M100, V101 – / F105, Y107	–/ M100, V101 F105/ F105
B’ helix	Y131, L134, T135, F139/ Y131	Y131, L134, T135, F139/ Y131	V130, Y131, L134, T135, F139/ –
B’’ η-turn	V143, A144, Y145/ –	V143, A144, Y145/ –	V143, A144, Y145/ –
C helix	F152, L159/ –	F152, L159/ –	F152, L159/ –
F’’	F234, S235, H236, W239/ L240	F234, S235, H236, W239/ L240	F234, S235, H236, W239/ L240, H236, W239
I	M304, G307, L308, L310, A311, T315/ –	M304, G307, L308, L310, A311, T315/ –	M304, G307, L308, L310, A311, T315/ –
K/β 1-4	I377, M381/ P375, P376, I377, M378, I379, M381	I377/ P376, I377, M381	I377, M381/ –
β1-3	– / –	–/ C402	Q400/ –
β4 hairpin	M487/ M487, I488, H489	M487/ M487, I488	/ Y484
Total contacts	24/ 18	21/ 15	24/ 12

Table S2. Data collection and refinement statistics.

Complex	Human CYP51- compound **10**
Data collection	
Wavelength, Å	0.0.9786
Space group	I4
Cell dimensions	
a, b, c, Å	117.764 117.764 157.842
α, β, γ, °	90.00, 90.00, 90.00
Molecules per asymmetric unit	2
Number of reflections	26405
Resolution (outer shell), Å	94.35 -2.80 (2.87-2.80)
R_{merge} (outer shell)	0.046 (0.996)
I/σ (outer shell)	12.3 (1.3)
Completeness (outer shell), %	99.6 (99.3)
Redundancy (outer shell)	5.6 (5.6)
Refinement	
R-work	0.227
R-free	0.255
Rms deviations from ideal geometry	
Bond lengths, Å	0.003
Bond angles, °	1.17
Ramachandran plot	
Residues in favorable/allowed regions, %	95.8/100
Outliers, %	0
Wilson B-factor	84.1
Number of atoms (mean B-factor, Å^2)	7658 (95.6)
Number of residues per molecule	A/B
Protein (mean B-factor, Å^2)	444/444 (101.5/98.4)
Heme (mean B-factor, Å^2)	1/1 (77.6/78.1)
Ligand (mean B-factor, Å^2)	**2/1** 101.8(116.7)/103.0)
Water (mean B-factor, Å^2)	30 (66.6)
PDB code	**6Q2T**

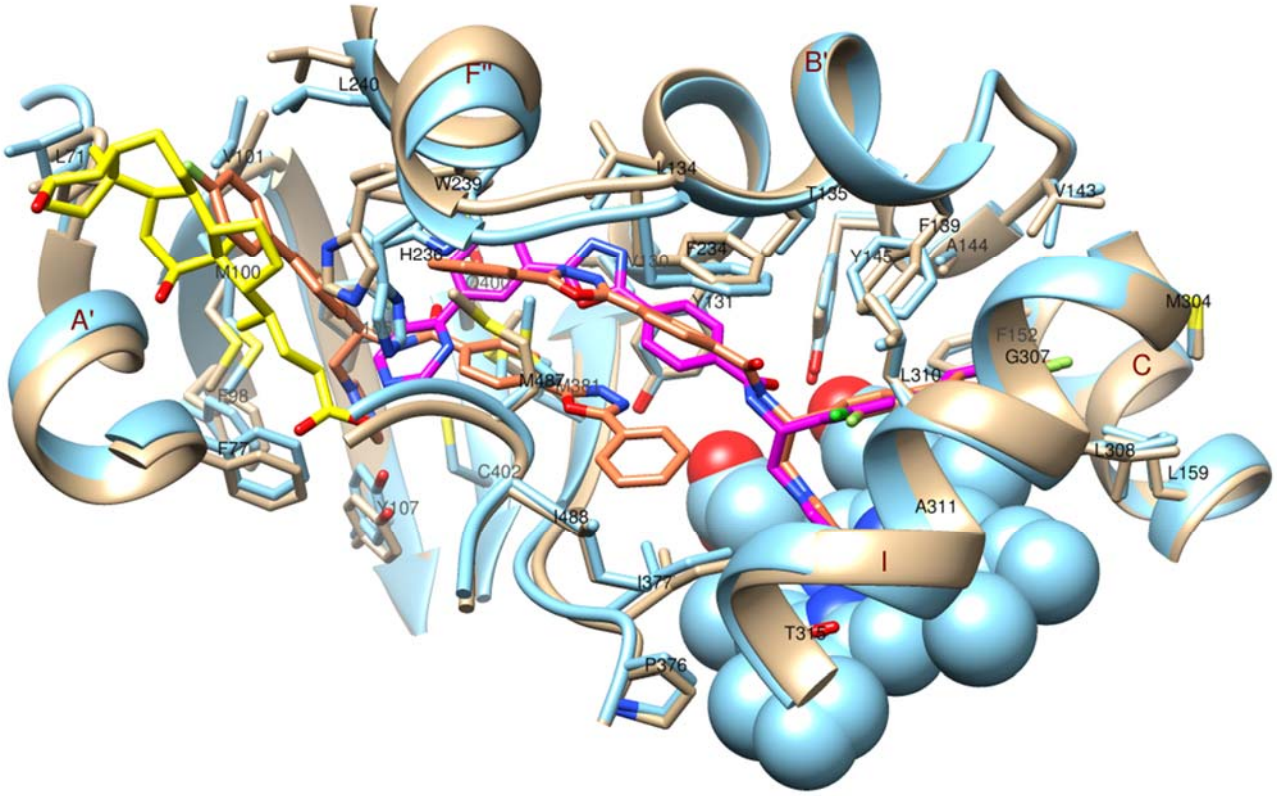

Supporting Figure S6. Active site forming secondary structural elements and ligand contacting residues in the superimposed compound 10-bound (blue) and VFV-bound (tan) human CYP51 structures.

Figure S7. HRMS spectra.

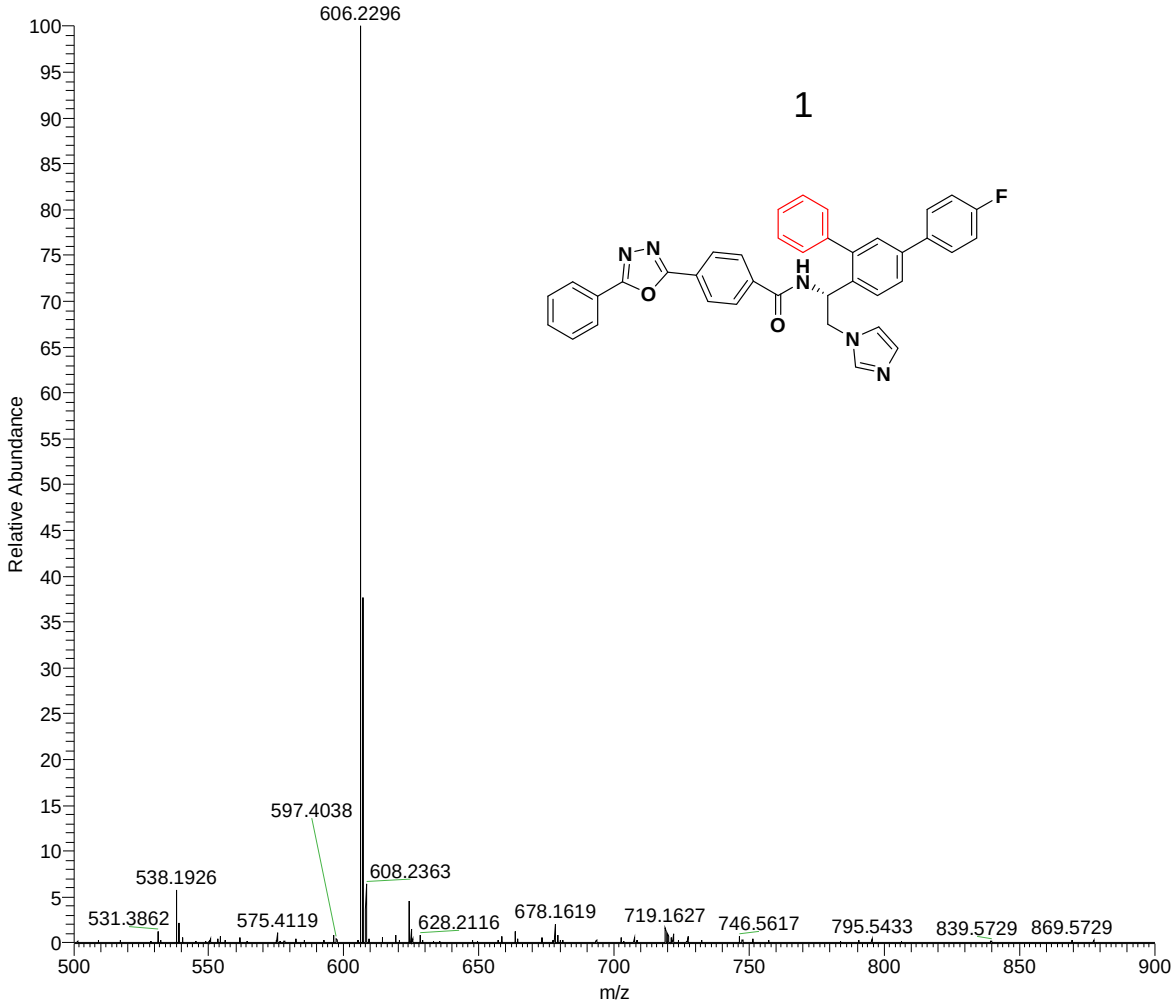

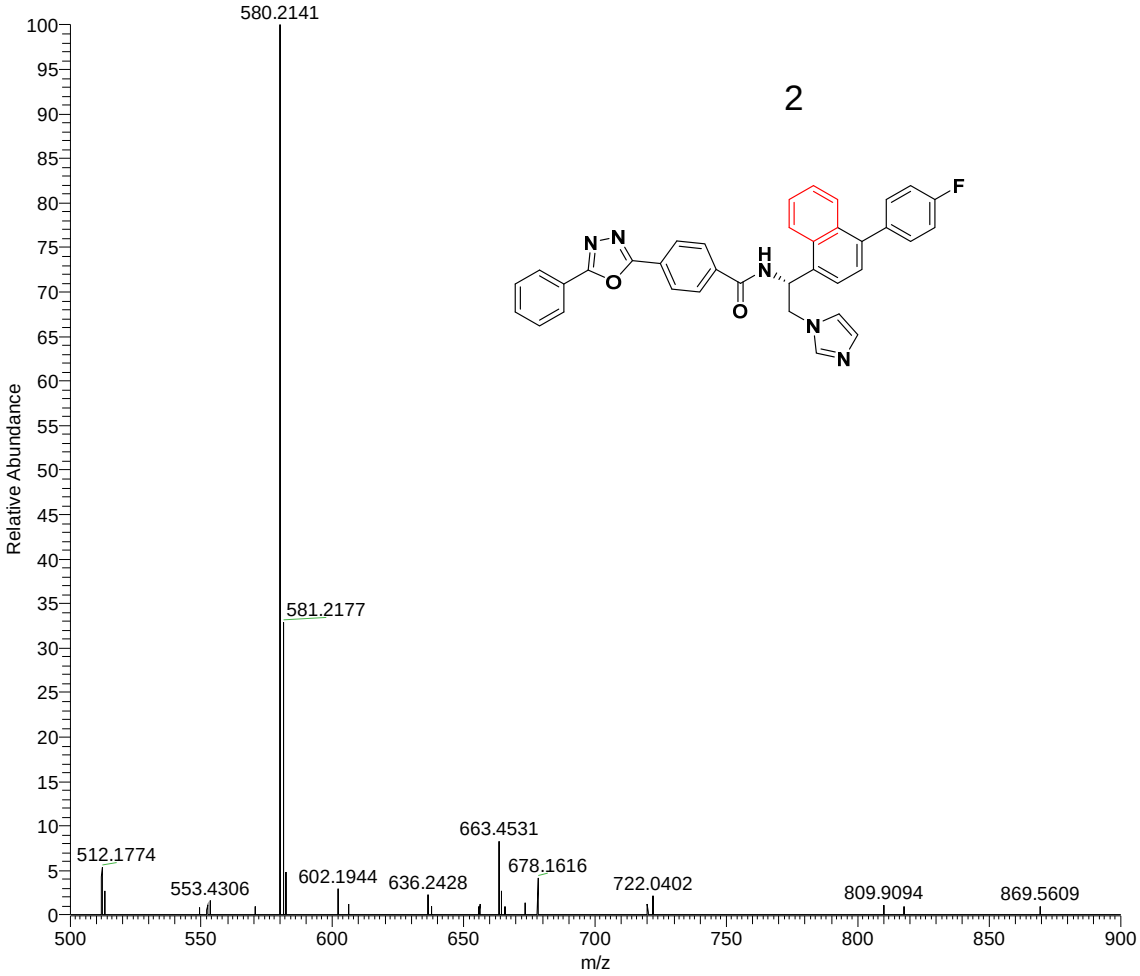
580.2141
581.2177
512.1774
553.4306
602.1944
636.2428
663.4531
678.1616
722.0402
809.9094
869.5609
Relative Abundance
m/z
2
F
N
O
H
N
O
N
N

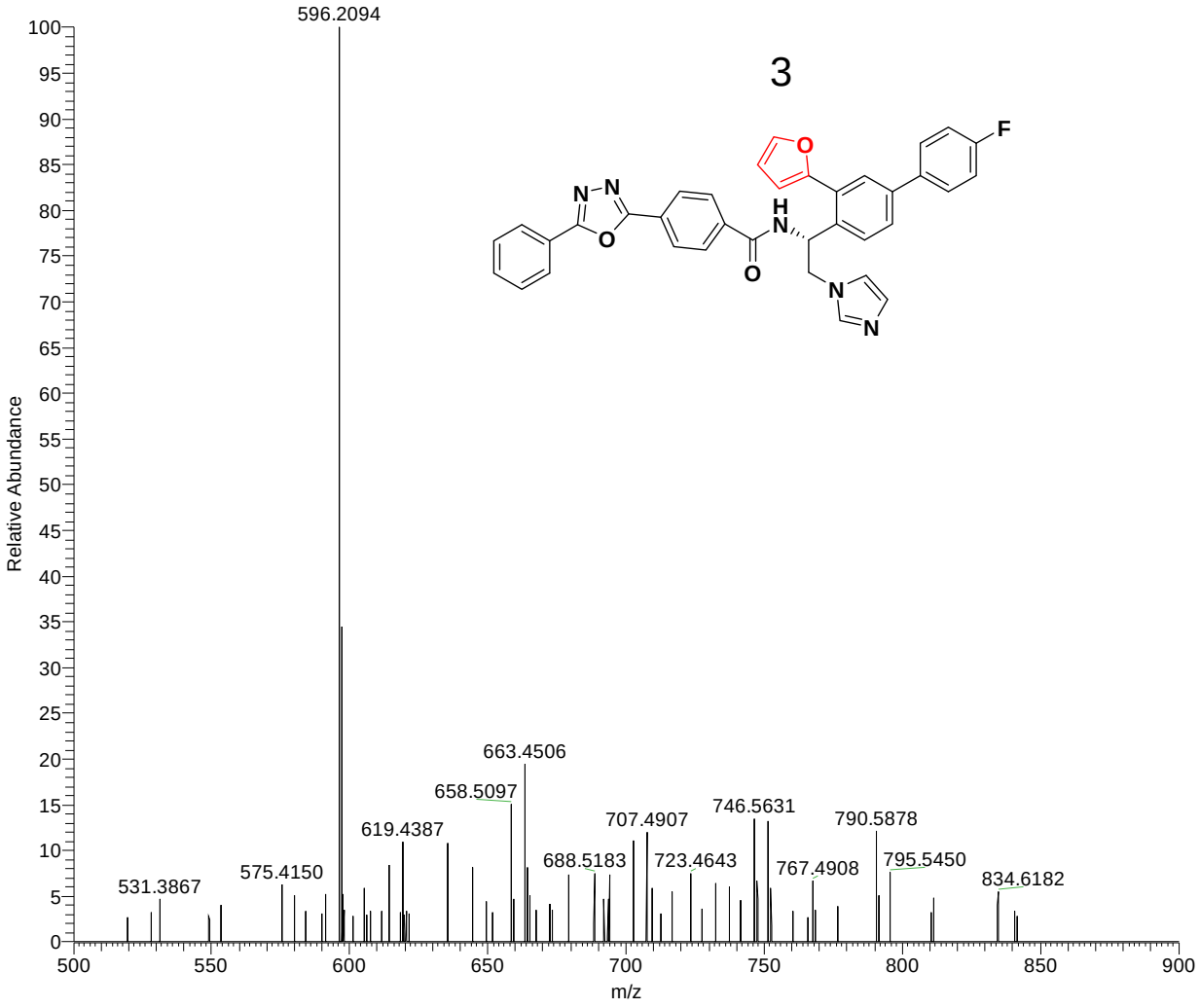
3
596.2094
663.4506
658.5097
746.5631
707.4907
790.5878
619.4387
688.5183
723.4643
795.5450
767.4908
575.4150
531.3867
834.6182
Relative Abundance
m/z

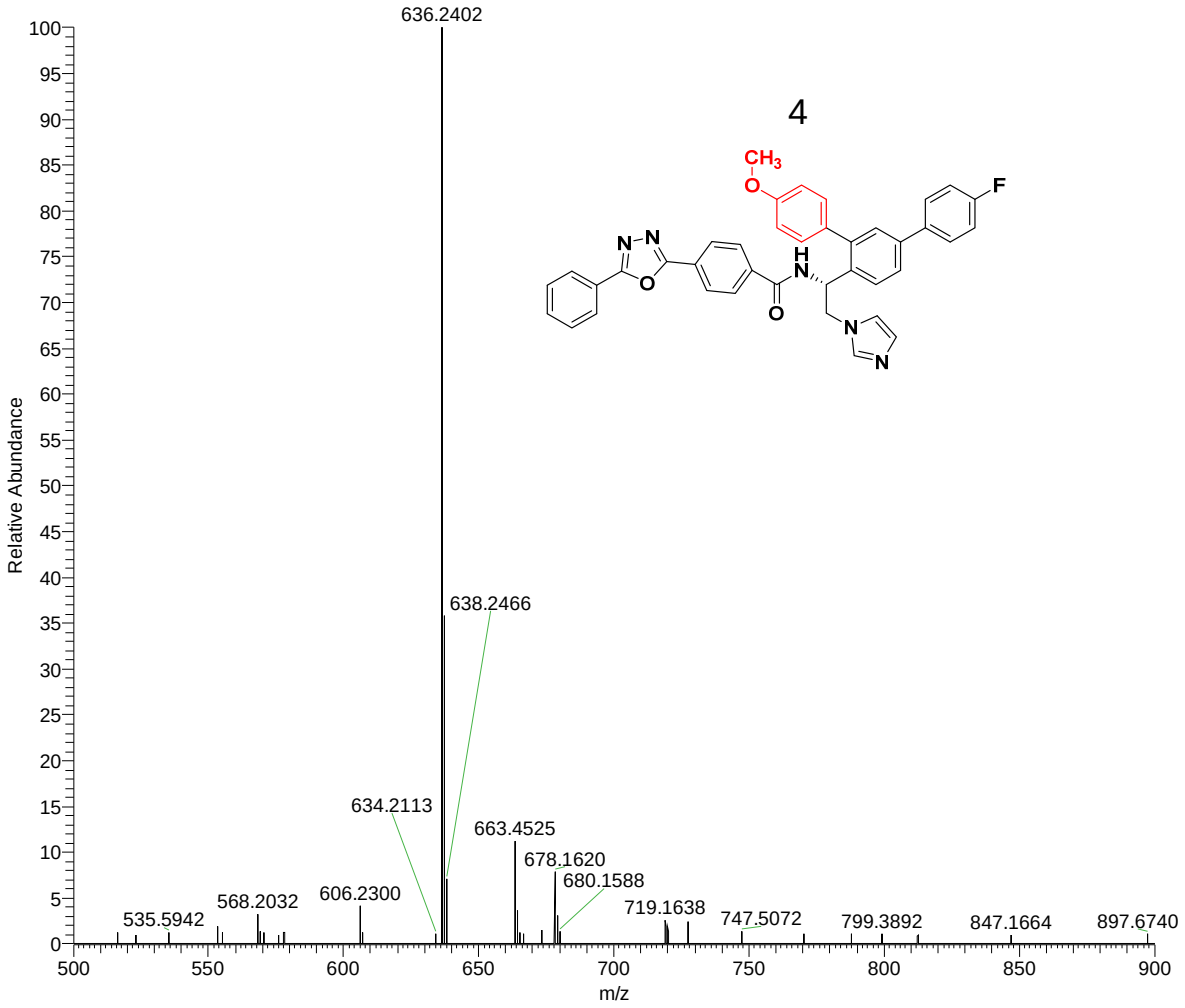
4
636.2402
638.2466
634.2113
663.4525
678.1620
680.1588
719.1638
747.5072
799.3892
847.1664
897.6740
606.2300
568.2032
535.5942
Relative Abundance
m/z

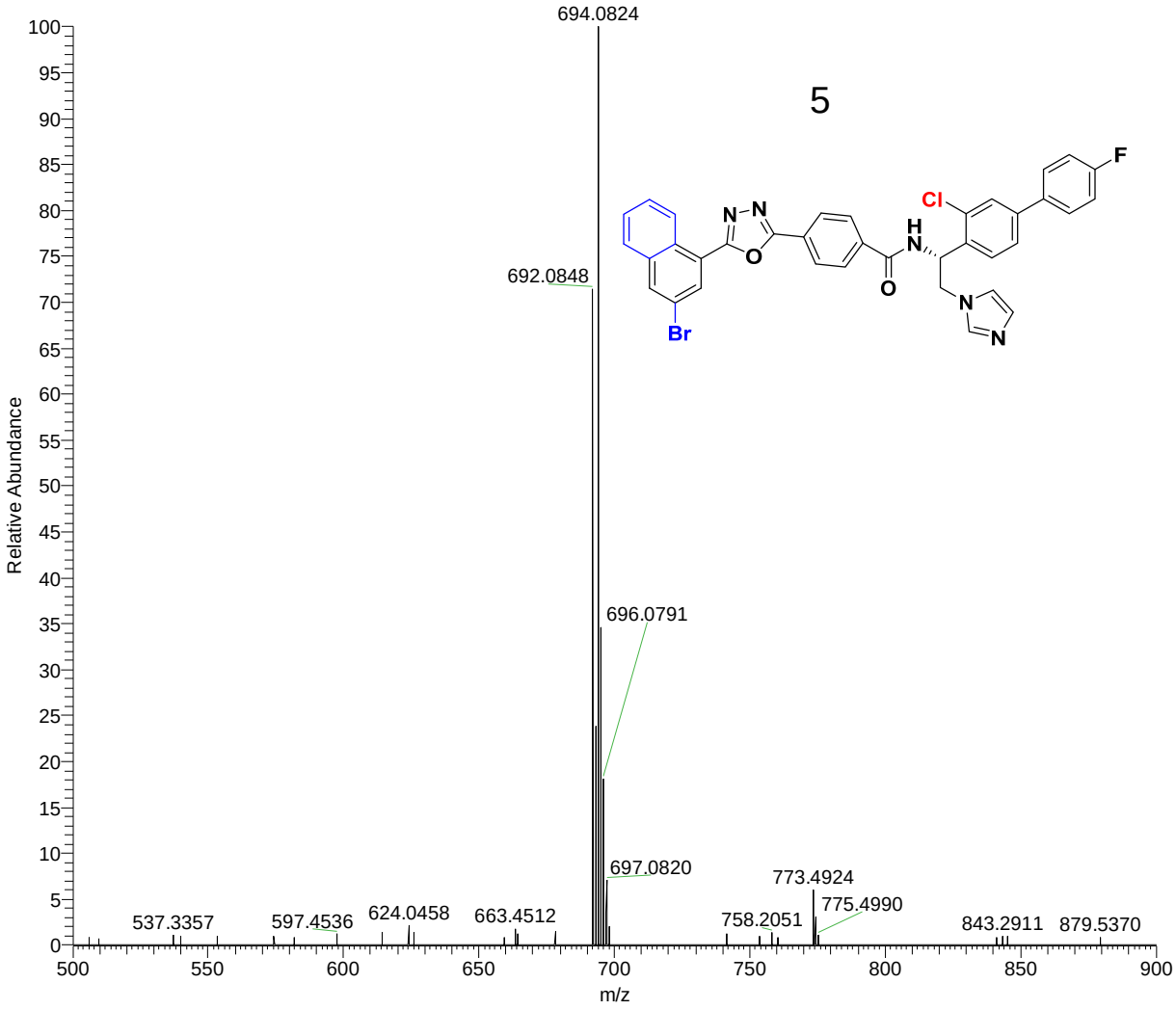
694.0824
692.0848
696.0791
697.0820
773.4924
775.4990
537.3357
597.4536
624.0458
663.4512
758.2051
843.2911
879.5370
Relative Abundance
m/z
5
Br
N
O
H
N
Cl
F
O
N
N

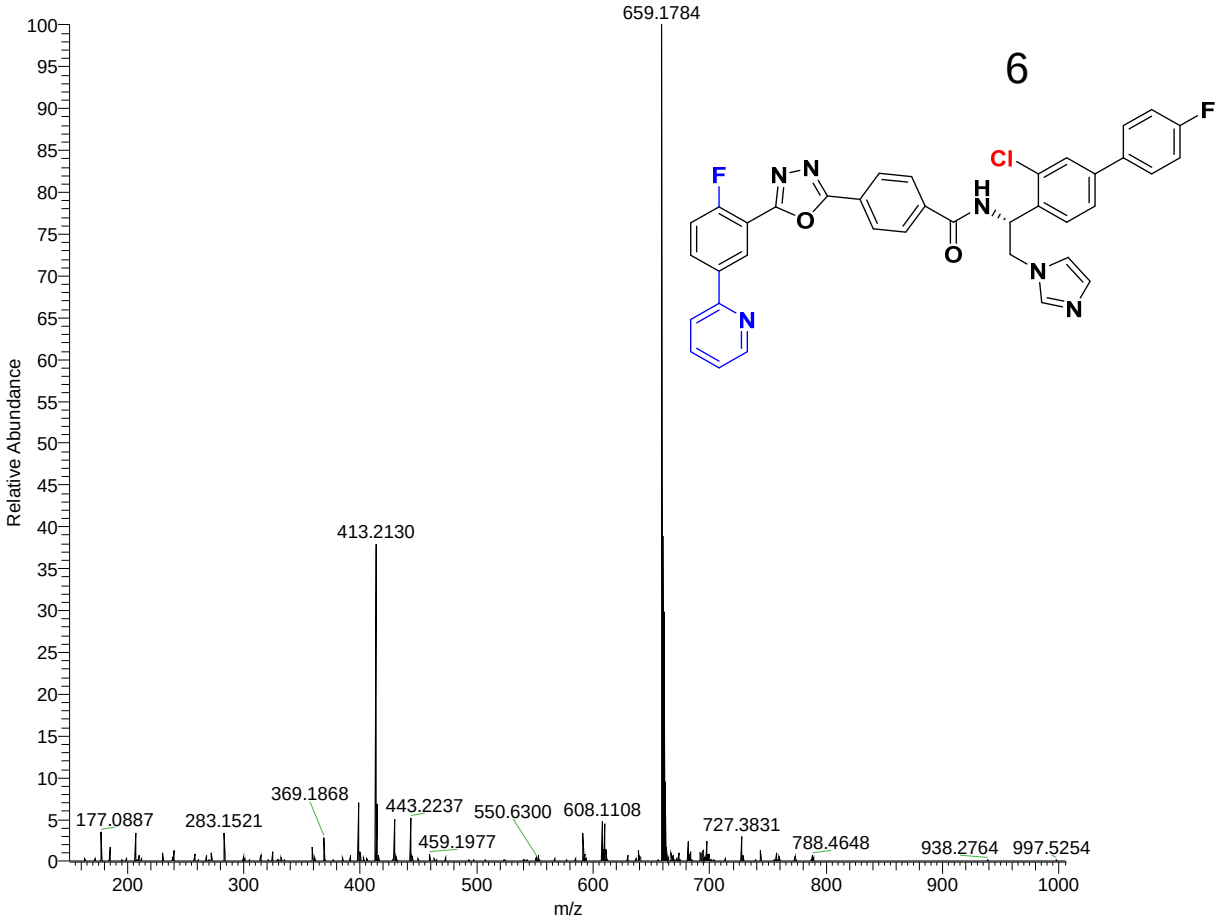
659.1784
6
413.2130
369.1868
443.2237
550.6300
608.1108
177.0887
283.1521
459.1977
727.3831
788.4648
938.2764
997.5254
Relative Abundance
m/z

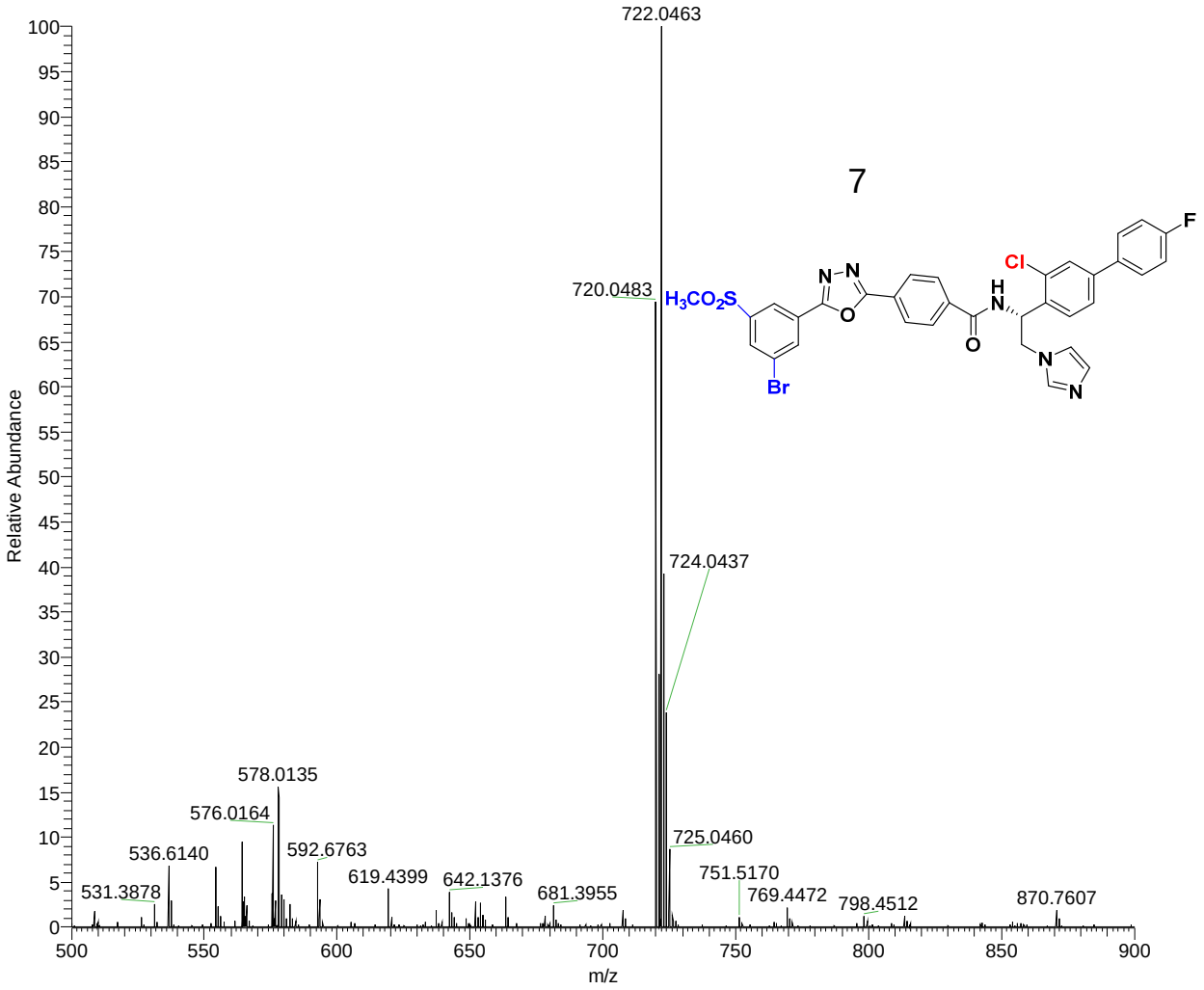
722.0463
720.0483
724.0437
578.0135
576.0164
536.6140
592.6763
619.4399
642.1376
681.3955
725.0460
751.5170
769.4472
798.4512
870.7607
531.3878
Relative Abundance
m/z
7
H_3CO_2S
Br
Cl
F
O
N
H

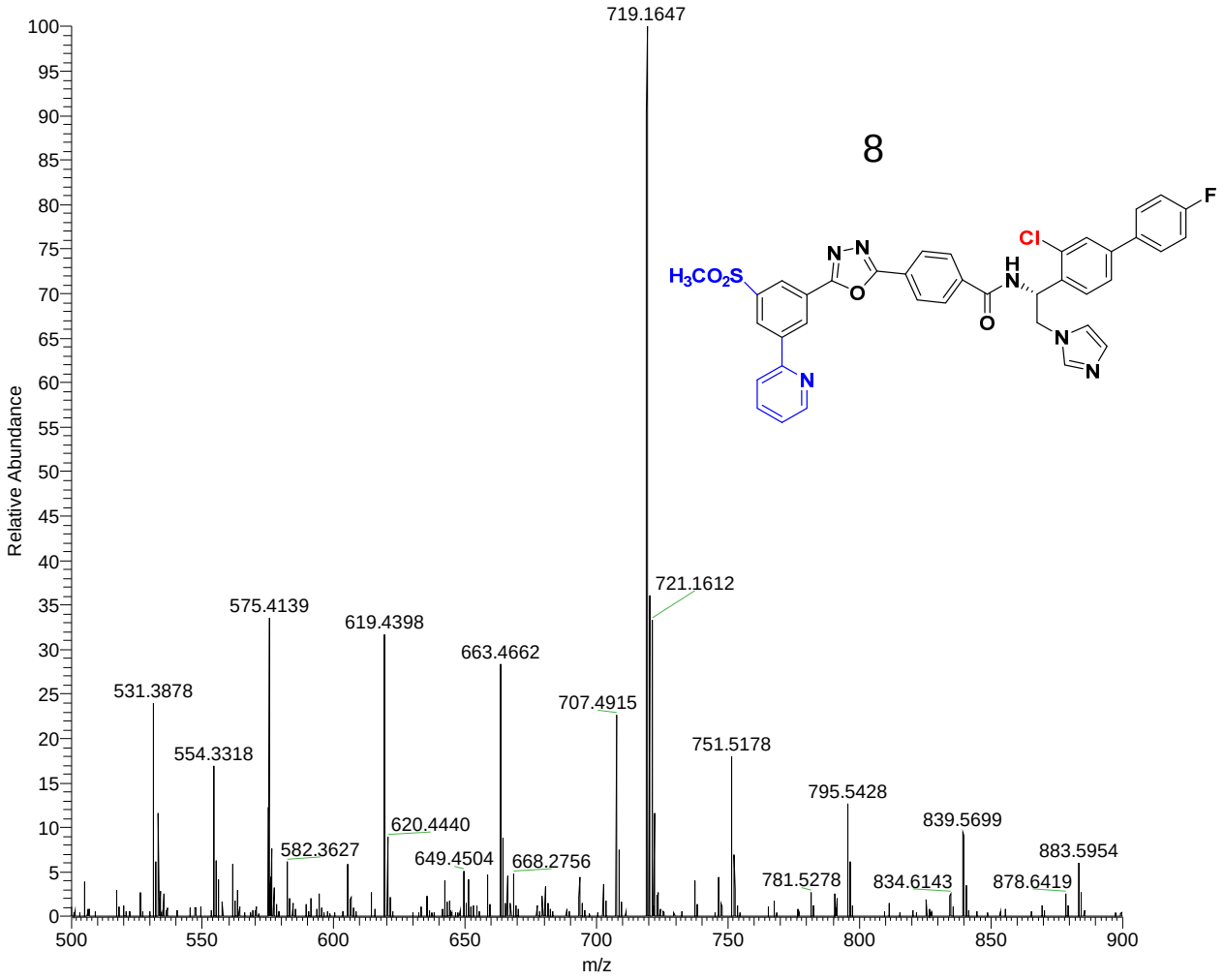
8
719.1647
721.1612
575.4139
619.4398
663.4662
531.3878
707.4915
554.3318
751.5178
795.5428
839.5699
620.4440
582.3627
649.4504
668.2756
781.5278
834.6143
878.6419
883.5954
Relative Abundance
m/z
H3CO2S
Cl
F

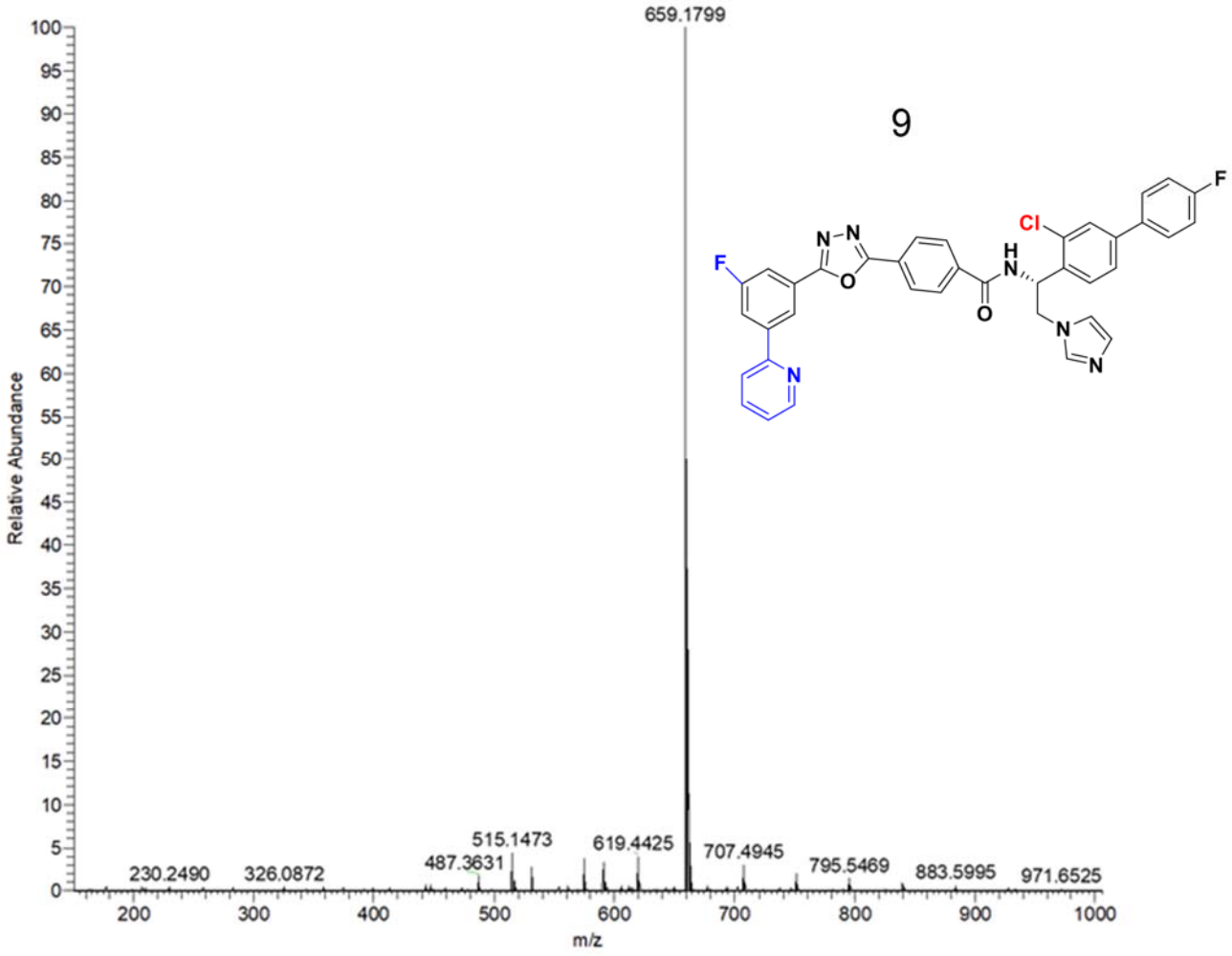
659.1799
9
Relative Abundance
m/z
230.2490
326.0872
487.3631
515.1473
619.4425
707.4945
795.5469
883.5995
971.6525
F
Cl
F
N
N
O
H
N
O
N
N

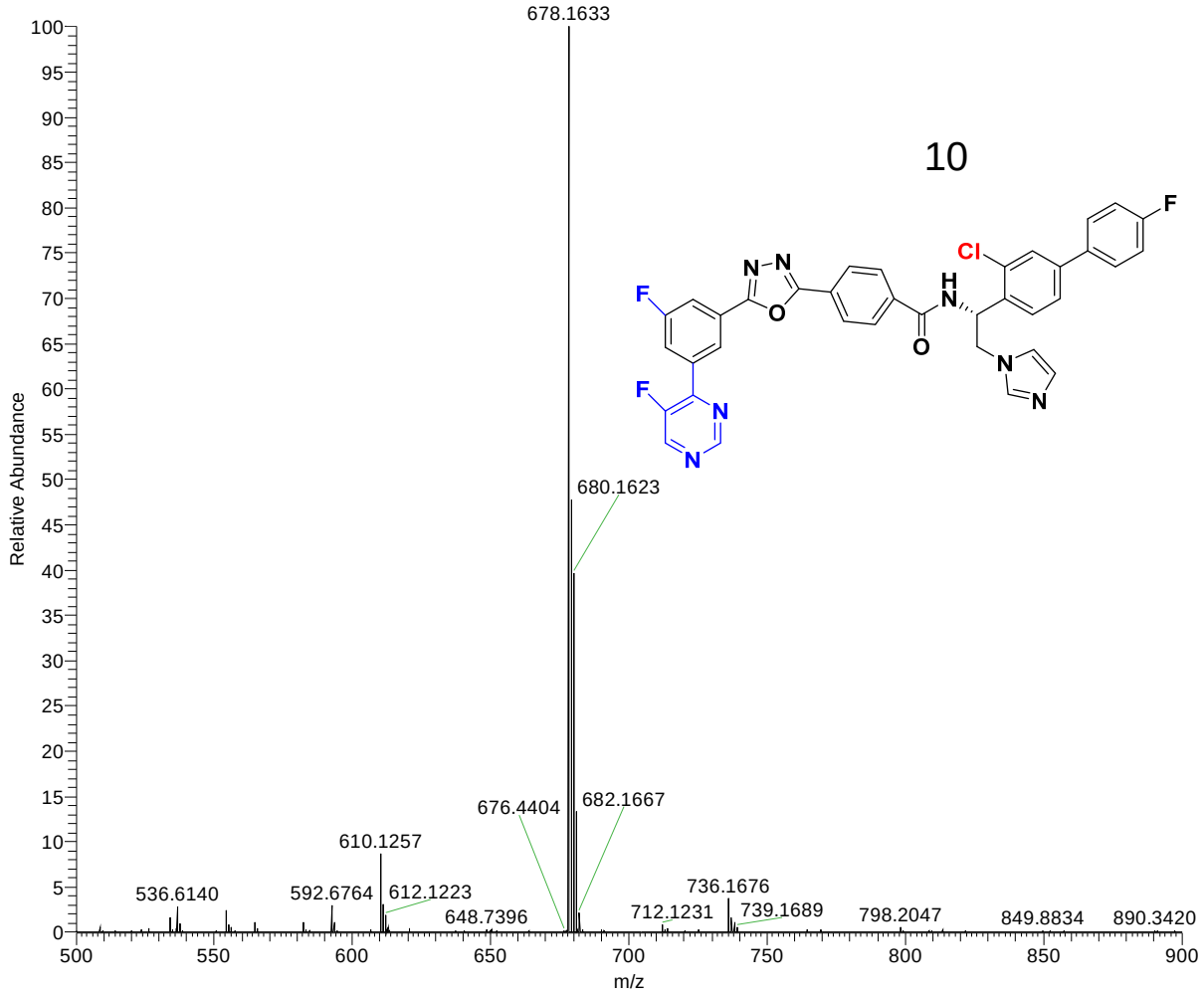
678.1633
680.1623
676.4404
682.1667
610.1257
536.6140
592.6764
612.1223
648.7396
712.1231
736.1676
739.1689
798.2047
849.8834
890.3420
Relative Abundance
m/z
10
F
Cl
N
N
O
H
N
O
F
F
N
N
N
N

Figure S8. ^{1}H NMR spectra.

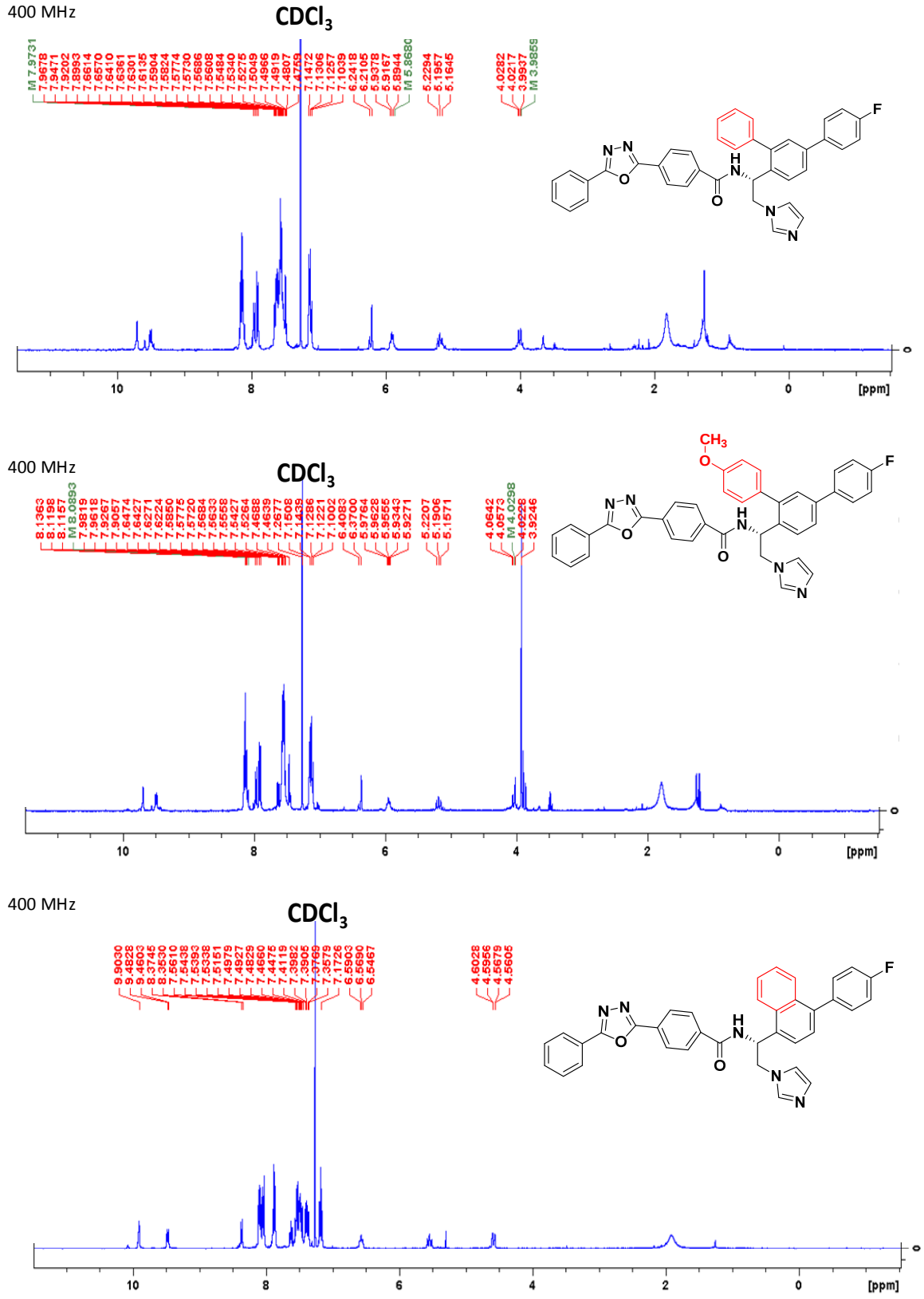

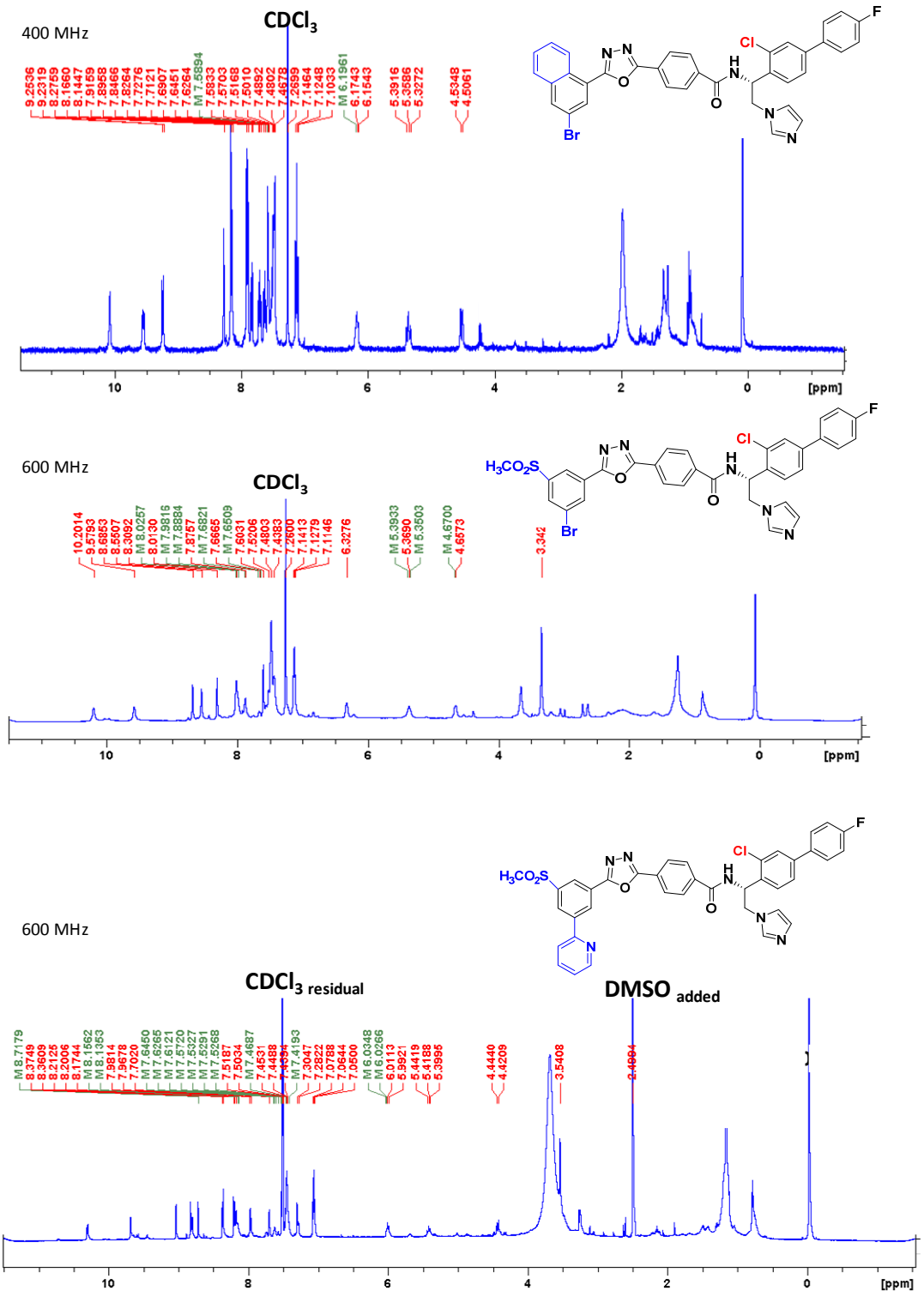

The compound was not soluble in $CDCl_3$, and one drop of DMSO-*d6* was added to the solution

600 MHz

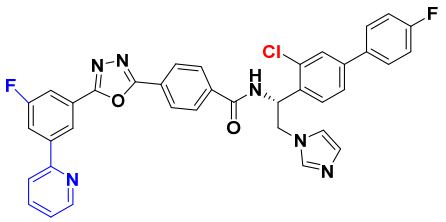

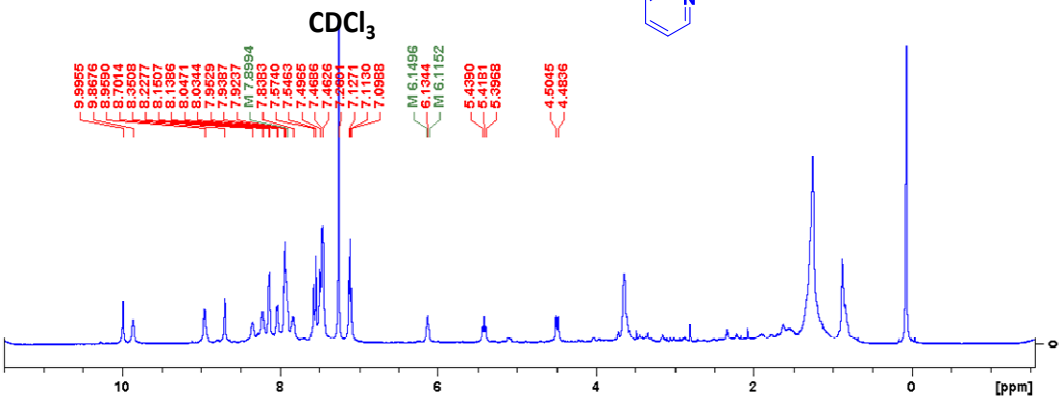

600 MHz

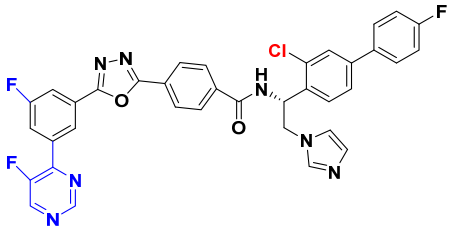

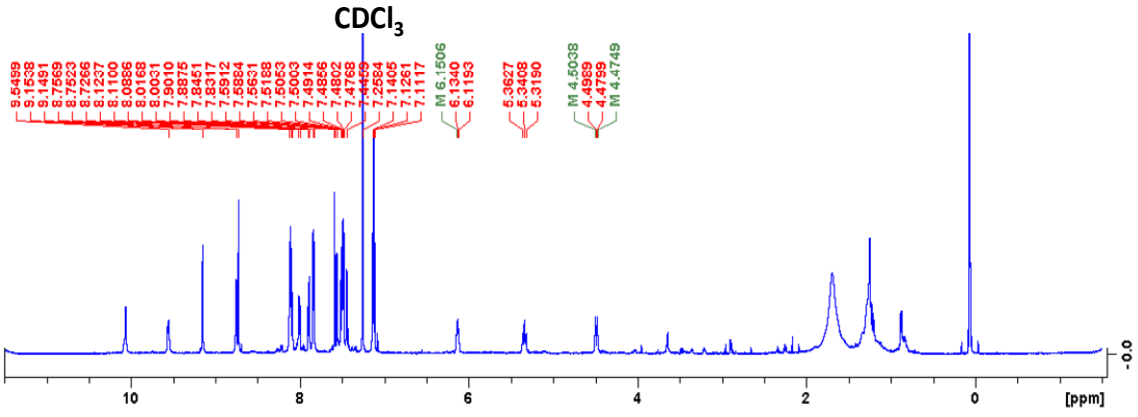

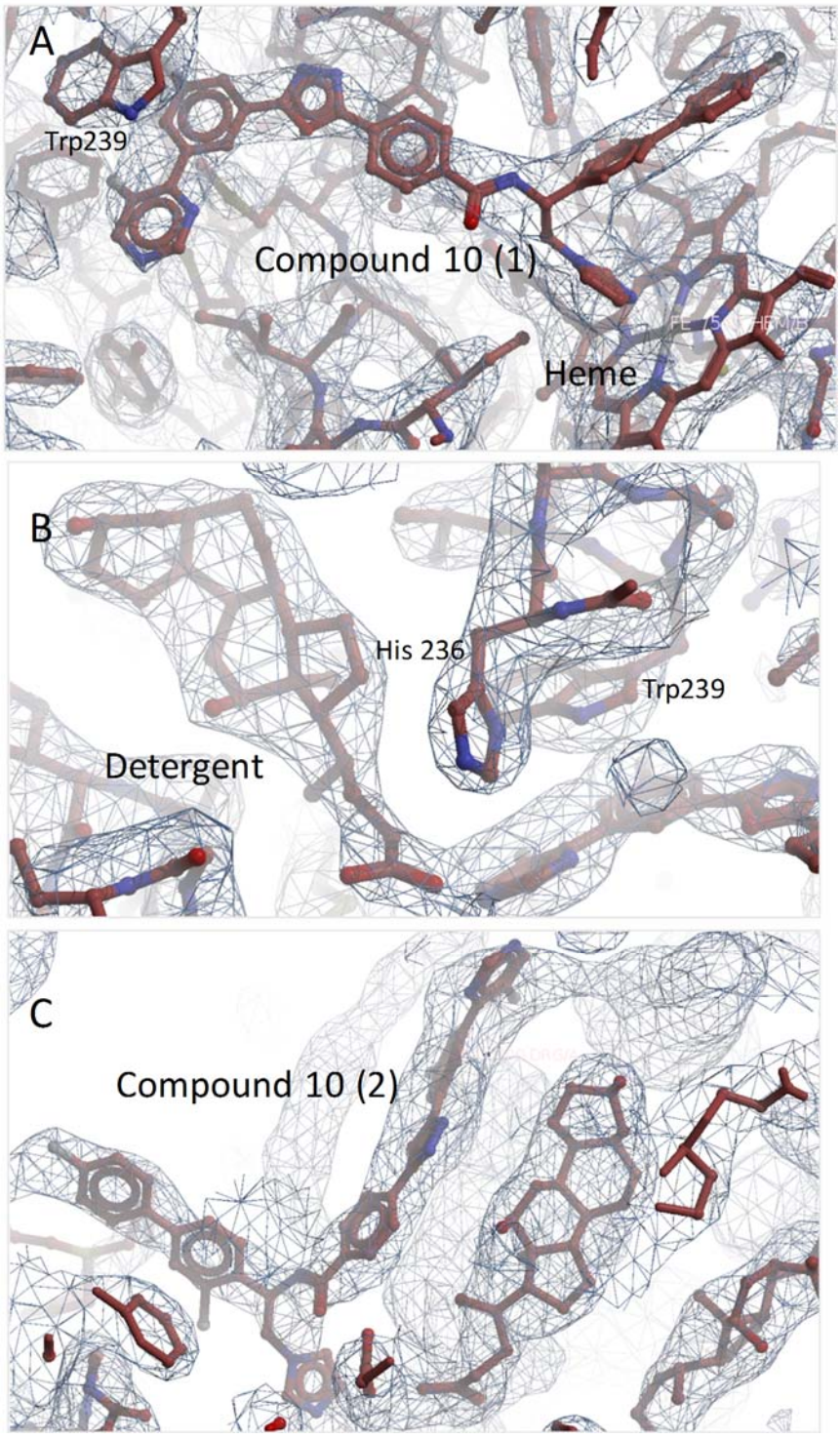

Figure S9. The 2Fo-Fc electron density maps (1.5 σ) for (A) the heme-coordinated inhibitor, (B) the active site entering deoxycholate, and (C) the run-away inhibitor.